Journal of Nuclear Medicine, published on September 21, 2023 as doi:10.2967/jnumed.123.266007

# Tumor-Targeted Interleukin 2 Boosts the Anticancer Activity of FAP-Directed Radioligand Therapeutics

Andrea Galbiati*[1], Paulina Dorten*[2], Ettore Gilardoni[1], Florian Gierse[2], Matilde Bocci[1], Aureliano Zana[1], Jacqueline Mock[1], Michael Claesener[3], Juela Cufe[2,3], Florian Büther[3], Klaus Schäfers[2], Sven Hermann[2], Michael Schäfers[2–4], Dario Neri[5,6], Samuele Cazzamalli[1], and Philipp Backhaus[2–4]

[1]*Research and Development Department, Philochem AG, Otelfingen, Switzerland;* [2]*European Institute for Molecular Imaging, University of Münster, Münster, Germany;* [3]*Department of Nuclear Medicine, University Hospital Münster, Münster, Germany;* [4]*West German Cancer Centre, Münster, Germany;* [5]*Department of Chemistry and Applied Biosciences, Swiss Federal Institute of Technology, Zurich, Switzerland; and* [6]*Philogen S.p.A., Siena, Italy*

We studied the antitumor efficacy of a combination of $^{177}$Lu-labeled radioligand therapeutics targeting the fibroblast activation protein (FAP) (OncoFAP and BiOncoFAP) with the antibody–cytokine fusion protein L19-interleukin 2 (L19-IL2) providing targeted delivery of interleukin 2 to tumors. **Methods:** The biodistribution of $^{177}$Lu-OncoFAP and $^{177}$Lu-BiOncoFAP at different molar amounts (3 vs. 250 nmol/kg) of injected ligand was studied via SPECT/CT in mice bearing subcutaneous HT-1080.hFAP tumors, and self-absorbed tumor and organ doses were calculated. The in vivo anticancer effect of 5 MBq of the radiolabeled preparations was evaluated as monotherapy or in combination with L19-IL2 in subcutaneously implanted HT-1080.hFAP and SK-RC-52.hFAP tumors. Tumor samples from animals treated with $^{177}$Lu-BiOncoFAP, L19-IL2, or both were analyzed by mass spectrometry–based proteomics to identify therapeutic signatures on cellular and stromal markers of cancer and on immunomodulatory targets. **Results:** $^{177}$Lu-BiOncoFAP led to a significantly higher self-absorbed dose in FAP-positive tumors (0.293 ± 0.123 Gy/MBq) than did $^{177}$Lu-OncoFAP (0.157 ± 0.047 Gy/MBq, $P = 0.01$) and demonstrated favorable tumor-to-organ ratios at high molar amounts of injected ligand. Administration of L19-IL2 or $^{177}$Lu-BiOncoFAP as single agents led to cancer cures in only a limited number of treated animals. In $^{177}$Lu-BiOncoFAP–plus–L19-IL2 combination therapy, complete remissions were observed in all injected mice (7/7 complete remissions for the HT-1080.hFAP model, and 4/4 complete remissions for the SK-RC-52.hFAP model), suggesting therapeutic synergy. Proteomic studies revealed a mechanism of action based on the activation of natural killer cells, with a significant enhancement of the expression of granzymes and perforin 1 in the tumor microenvironment after combination treatment. **Conclusion:** The combination of OncoFAP-based radioligand therapeutics with concurrent targeting of interleukin 2 shows synergistic anticancer effects in the treatment of FAP-positive tumors. This experimental finding should be corroborated by future clinical studies.

**Key Words:** combination therapies; fibroblast activation protein; immunocytokines; radioligand therapeutics; tumor targeting

**J Nucl Med 2023; 64:1–7**
DOI: 10.2967/jnumed.123.266007

The fibroblast activation protein (FAP) is one of the most attractive and studied targets for radiotheranostic applications (*1*). FAP is found at high concentrations in the tumor microenvironment of many types of human malignancies (*2*) and on the cell surface of specific sarcoma subtypes (*3,4*). Suboptimal biodistribution profiles have been reported using radiolabeled preparations of FAP-specific antibodies (*5*). In contrast, nuclear medicine studies validated the use of small organic ligands and peptides to target FAP in solid tumor lesions (*2,6,7*). We have previously described the development of ultra-high-affinity FAP ligands (i.e., OncoFAP and BiOncoFAP; Philochem AG) for the delivery of cytotoxic and radioactive payloads to solid tumors (*8–11*).

Although cancer cures can be obtained in mice treated with radioligand therapeutics (RLTs) targeting prostate-specific membrane antigen (*12*), somatostatin receptor 2 (*13*), and FAP (*11,14–16*), complete remissions are rarely observed in cancer patients (*17,18*). For this reason, combination modalities that synergize with tumor-targeted RLTs are being investigated (*19*). The use of conventional chemotherapy (*20*), immune checkpoint inhibitors (anti–programmed death 1, anti–programmed death ligand 1, anti–cytotoxic T lymphocyte antigen 4) (*21,22*), hedgehog inhibitors (*23*), DNA-repair inhibitors, poly(adenosine diphosphate ribose)polymerase inhibitors (*24*), heat shock protein 90 inhibitors (*25,26*), and topoisomerase I inhibitors (*27,28*) has been proposed as a strategy to sensitize tumors to the effect of targeted and nontargeted radioactive therapy. Although preclinical evidence demonstrates the validity of these approaches, only a few of these combination modalities have been successfully translated in clinical trials (*20,27,29*).

In this study, we investigated a novel combination strategy based on $^{177}$Lu-labeled OncoFAP RLTs and immunotherapy via L19-interleukin 2 (L19-IL2), a clinical-stage immunocytokine targeting the fibronectin extradomain B for the active delivery of interleukin 2 to subendothelial blood vessels in solid tumor lesions (*30*). We investigated whether locally delivered interleukin 2—via activation of natural killer (NK) cells and T cells—synergistically enhances the antitumor effect of FAP-directed RLTs. Similarly to FAP, the alternatively spliced extradomain B of fibronectin is a stromal tumor–associated antigen that is expressed in most malignancies while being virtually undetectable in normal tissues (*31*). The antigen is completely conserved from mice to humans and shows a pattern of expression in the tumor neovasculature and in the extracellular matrix (*30,31*). Synergy of tumor-targeted interleukin 2 with other therapeutic modalities, including conventional chemotherapy (*32*),

Received May 8, 2023; revision accepted Aug. 18, 2023.
For correspondence or reprints, contact Samuele Cazzamalli (samuele.cazzamalli@philochem.ch) or Philipp Backhaus (philipp.backhaus@ukmuenster.de).
*Contributed equally to this work.
Published online Sep. 21, 2023.

targeted cytotoxics (*9,33*), check-point inhibitors (*34–36*), other immunocytokines (*34,37,38*), and chimeric antigen receptor T cells (University of Muenster, unpublished data, 2015), have been previously demonstrated. Synergy with radiotherapies (*36,39,40*) that are currently being evaluated in a phase 2 study (*41*) provided a strong rationale for combining L19-IL2 with radioligand therapeutics based on β-emitters such as $^{177}$Lu.

## MATERIALS AND METHODS

L19-IL2 was provided by Philogen S.p.A. (the aminoacidic sequence is reported in Supplemental Table 1; supplemental materials are available at http://jnm.snmjournals.org). $^{177}$Lu (no carrier added) was purchased from ITM Radiopharma.

### Chemistry and Radiochemistry

OncoFAP-DOTAGA and BiOncoFAP-DOTAGA were synthesized as previously described (*9,11*). Radiolabeling with $^{177}$Lu is outlined in the supplemental materials. Different molar amount preparations were generated by adding defined amounts of precursor compound solution after radiolabeling.

### Cell Culture

The FAP-transfected cell lines SK-RC-52.hFAP and HT-1080.hFAP were generated following the protocol described by Millul et al. (*9*). Briefly, SK-RC-52 (renal cell carcinoma; Memorial Sloan Kettering Cancer Center) and HT-1080 (fibrosarcoma; ATCC) cell lines were seeded in 24-well plates and incubated with a lentiviral system containing cloned hFAP transgene (*9*). Cells were grown and expanded for 3 wk, and positive cells were sorted at the flow cytometry facility (FACSArial III; BD Biosciences) using FAP phycoerythrin-conjugated antibody (R&D Systems).

SK-RC-52.hFAP tumor cells were grown to 80% confluence in RPMI-1640 medium. HT-1080.hFAP and HT-1080 wild-type (HT-1080.wt) tumor cells were grown to 95% confluence in Dulbecco modified Eagle medium. All cell lines were cultured with 10% fetal bovine serum and 1% antibiotic–antimycotic and detached with trypsin–ethylenediaminetetraacetic acid, 0.05%.

### Animal Studies

All animal experiments with SK-RC-52.hFAP tumor cells were conducted in accordance with Swiss animal welfare laws and regulations under license ZH006/2021 granted by the Veterinäramt des Kantons Zürich. Animals studies involving the use of HT-1080 tumor cells were conducted in accordance with the German Law on the Care and Use of Laboratory Animals and approved by the Landesamt für Natur, Umwelt, und Verbraucherschutz of North Rhine–Westphalia, Germany.

### Implantation of Subcutaneous Tumors

SK-RC-52.hFAP, HT-1080.hFAP, or HT-1080.wt cells were resuspended in Hanks balanced salt solution medium. Aliquots of 5 million cells (SK-RC-52.hFAP) or 2 million cells (HT-1080) in 100 μL of suspension were injected subcutaneously in the right flank (SK-RC-52.hFAP), in the left shoulder (HT-1080.hFAP), or in the right shoulder (HT-1080.wt) of female athymic BALB/c AnNRj-Foxn1 mice (6–9 wk old). Before biodistribution and therapy studies, the tumors were allowed to grow to about 100–200 mm$^3$.

### Quantitative Biodistribution and Dosimetry of $^{177}$Lu-OncoFAP and $^{177}$Lu-BiOncoFAP

Mice bearing bilateral subcutaneous tumors were imaged in a small-animal SPECT/CT system (nanoScan; Mediso) calibrated for $^{177}$Lu. At 10–13 d after implantation, the mice were intravenously injected with 5 MBq of $^{177}$Lu-OncoFAP ($n$ = 5) or $^{177}$Lu-BiOncoFAP (5 animals with 3 nmol/kg and 3 animals with 250 nmol/kg). SPECT images were acquired at approximately 15 min, 30 min, 45 min, 2.5 h, 24 h, and 96 h after injection followed by non–contrast-enhanced CT. After completion of the 96-h imaging, the mice were euthanized, organs and tumors were withdrawn, and the radioactivity was measured using a γ-counter (Perkin Elmer). For SPECT/CT analysis, representative ellipsoid or spheric volumes of interest for organs and voxelwise volumes of interest covering the entire tumors were drawn on the basis of the CT component of the SPECT/CT. For estimation of self-absorbed dose (or specific absorbed dose, expressed in Gy/MBq) in organs and tumors, time–activity curves of single animals were fitted according to the method of Jackson et al. using the scripted implementation (*42*). This involved using a model consisting of a triexponential function fitted to the latest 3 acquisitions. S values accounting for the geometric relationships of organs at nonuniform activity distributions were not considered.

### Therapy Studies with $^{177}$Lu-OncoFAP and $^{177}$Lu-BiOncoFAP in Tumor-Bearing Mice

Tumor-bearing mice were randomized and intravenously injected with $^{177}$Lu-OncoFAP, $^{177}$Lu-BiOncoFAP, or vehicle (7 animals with 250 MBq/kg at 3 nmol/kg for HT-1080.hFAP and 4 animals with 250 MBq/kg at 250 nmol/kg for SK-RC-52.hFAP). The mice were subcutaneously (HT-1080.hFAP) or intravenously (SK-RC-52.hFAP)

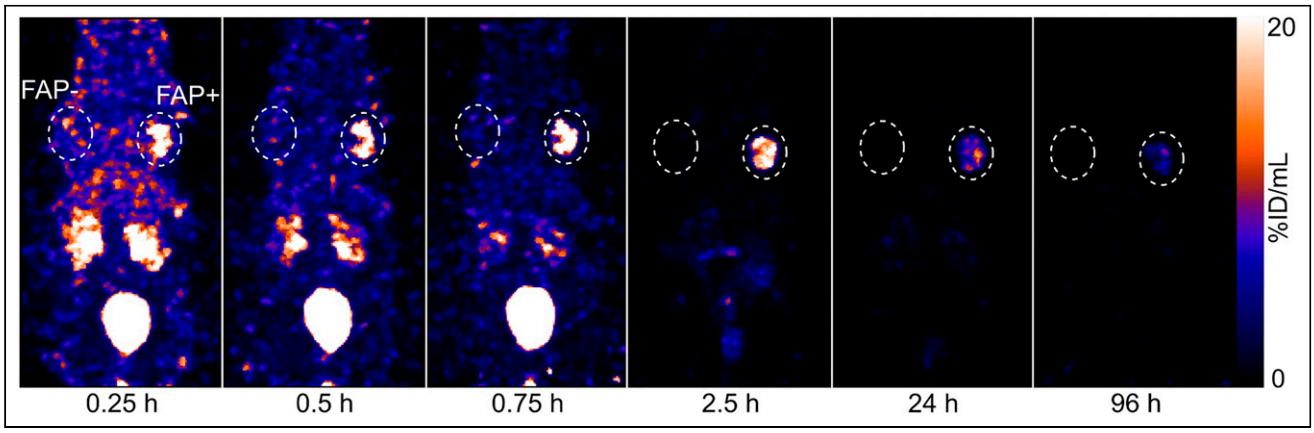


**FIGURE 1.** Example of longitudinal SPECT/CT maximal-intensity projections after injection of 5 MBq of $^{177}$Lu-BioncoFAP at 250 nmol/kg. Right-sided HT-1080.hFAP (FAP-positive) and left-sided HT-1080.wt (FAP-negative) subcutaneous tumors at shoulder are encircled. Supplemental Figure 1 provides visual comparison of SPECT/CT $^{177}$Lu-BioncoFAP and $^{177}$Lu-OncoFAP at 3 nmol/kg. %ID = percentage injected dose.

injected with a 2.5 mg/kg dose of L19-IL2 or vehicle. The schedule of combination in the 2 different models is based on our previous experience with L19-IL2 in combination with various therapeutic modalities (*9,32,33*). Animal body weight, stress score, and tumor size in 2 dimensions were acquired daily by investigators (masked). The mice were euthanized on termination criteria given by the animal testing license (i.e., a predefined stress score, tumor diameter ≥ 15 mm) 35 d (HT-1080.hFAP) or 25 d (SK-RC-52.hFAP) after implantation. Tumor volumes were calculated as length × width$^2$ × 0.5.

### Proteomic Analysis

SK-RC-52.hFAP tumor–bearing mice were treated with saline, $^{177}$Lu-BiOncoFAP, L19-IL2, or the combination of $^{177}$Lu-BiOncoFAP plus L19-IL2. The mice were euthanized on day 15 after tumor implantation (7 d after the initiation of therapeutic treatments) by $CO_2$ asphyxiation, and tumors were harvested and snap-frozen with liquid nitrogen. Tumor tissues were processed and analyzed as presented in the supplemental materials.

### Statistical Analysis

Statistical comparison of self-absorbed doses was performed using the Wilcoxon rank-sum test with Matlab software (version R2020a; MathWorks). *P* values of less than 0.05 were considered significant. No multiple-comparison corrections were performed; therefore, statics are considered descriptive. Statistical analysis for therapeutic outcomes and proteomics were performed with GraphPad Prism 8.

## RESULTS

### SPECT/CT-Based Biodistribution and Dosimetry

Longitudinal SPECT/CT was performed on mice bearing HT-1080.hFAP (left shoulder) and HT-1080.wt (right shoulder) tumors to gather time–activity curves for self-absorbed dose calculations. At high molar amounts (250 nmol/kg), $^{177}$Lu-BiOncoFAP demonstrated selective accumulation in FAP-positive tumors and rapid clearance from FAP-negative tumors and organs (Figs 1 and 2A; Supplemental Table 2). This led to calculated self-absorbed doses of 0.302 ± 0.060 Gy/MBq for FAP-positive tumors and low doses in FAP-negative tumors (0.005 ± 0.001 Gy/MBq) or organs such as the liver (0.018 ± 0.010 Gy/MBq) or bones (0.002 ± 0.001 Gy/MBq) (Fig. 2B; Supplemental Table 3). Uptake and dose values for tumors were probably underestimated given the tendency of some tumors to develop necrosis (Supplemental Fig. 1). At low molar amounts (3 nmol/kg), $^{177}$Lu-BiOncoFAP uptake kinetics and self-absorbed dose in FAP-positive tumors matched results obtained at 250 nmol/kg (0.287 ± 0.149 Gy/MBq, $P$ = 0.571) (Fig. 2B; Supplemental Figs. 2 and 3). In contrast, uptake, retention, and self-absorbed dose were fundamentally higher for the low-molar-amount preparation in FAP-negative tumors (0.137 ± 0.007 Gy/MBq, $P$ = 0.036) and healthy organs such as the liver (0.376 ± 0.036, $P$ = 0.036) or joints and bones (0.081 ± 0.008 Gy/MBq, $P$ = 0.036). $^{177}$Lu-OncoFAP at 3 nmol/kg demonstrated approximately half as much self-absorbed dose in FAP-positive tumors (0.157 ± 0.047 Gy/MBq) as did $^{177}$Lu-BiOncoFAP (0.293 ± 0.123 Gy/MBq, $P$ = 0.01), because of the former's shorter tumor retention time.

### Evaluation of In Vivo Therapeutic Efficacy of OncoFAP-RTLs in Combination with L19-IL2

The therapeutic efficacy of 5 MBq of $^{177}$Lu-OncoFAP and of $^{177}$Lu-BiOncoFAP as monotherapy or in combination with L19-IL2 was assessed at low molar amounts of injected compound (3 nmol/kg) in mice bearing HT-1080.hFAP tumors and at high amounts (250 nmol/kg) in mice bearing SK-RC-52.hFAP tumors (Fig. 3).

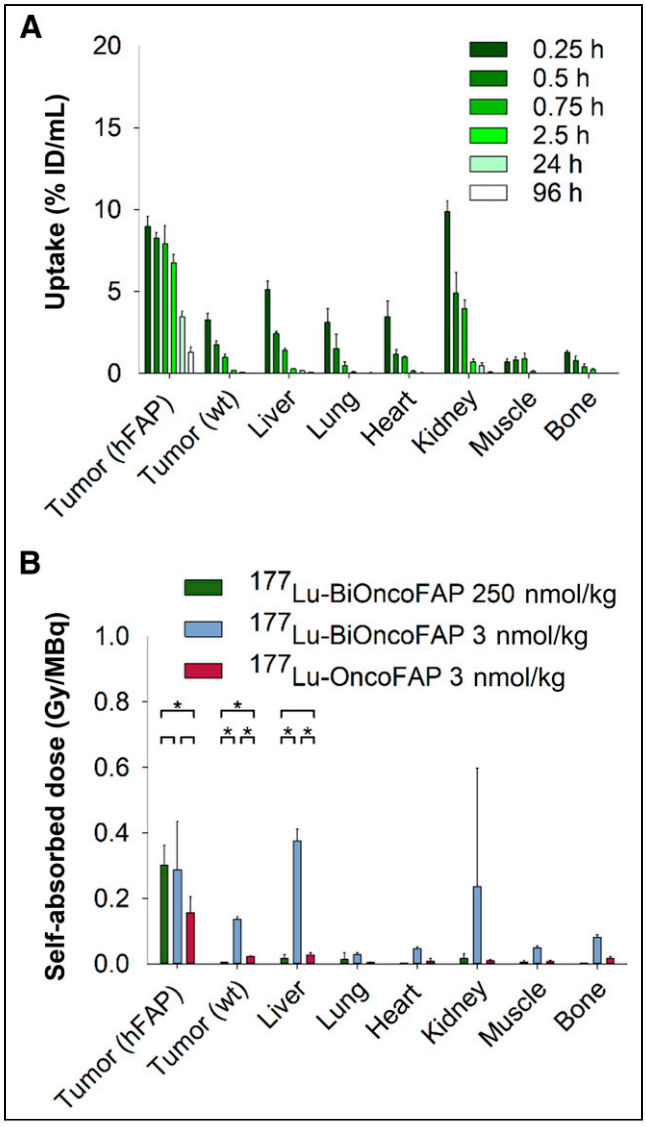


**FIGURE 2.** (A) SPECT/CT-derived uptake in HT-1080.hFAP and HT-1080.wt tumors and in organs of 3 mice after injection of 5 MBq of $^{177}$Lu-BioncoFAP at 250 nmol/kg. Supplemental Figure 3 and Supplemental Table 2 compare SPECT/CT-based biodistribution of $^{177}$Lu-BioncoFAP at 250 nmol/kg and $^{177}$Lu-BioncoFAP and $^{177}$Lu-OncoFAP at 3 nmol/kg. (B) Calculated self-absorbed doses for tumors and organs. Supplemental Table 3 provides all dose values and statistical comparisons. *$P$ < 0.05. %ID = percentage injected dose.

Untreated mice (saline group) bearing HT-1080.hFAP and SK-RC-52.hFAP tumors had to be euthanized after 14 and 16 d, respectively. At these time points, tumor volumes were 404 ± 222 mm$^3$ and 453 ± 42 mm$^3$, respectively. Therapy with $^{177}$Lu-OncoFAP resulted in minor tumor growth retardation in both models (HT-1080.hFAP, 153 ± 205 mm$^3$; SK-RC-52.hFAP, 202 ± 47 mm$^3$). Similar efficacy was observed for L19-IL2 monotherapy (HT-1080.hFAP, 286 ± 295 mm$^3$; SK-RC-52.hFAP, 152 ± 113 mm$^3$). Administration of $^{177}$Lu-BiOncoFAP resulted in a more potent antitumor effect (HT-1080.hFAP, 106 ± 151 mm$^3$; SK-RC-52.hFAP, 79 ± 55 mm$^3$), with 2 of 7 and 1 of 4 complete remissions, respectively. Combining L19-IL2 with $^{177}$Lu-OncoFAP potently boosted the antitumor activity, with 6 of 7 and 1 of 4 complete remissions. The highest efficacy was observed for L19-IL2 plus $^{177}$Lu-BiOncoFAP, with complete tumor

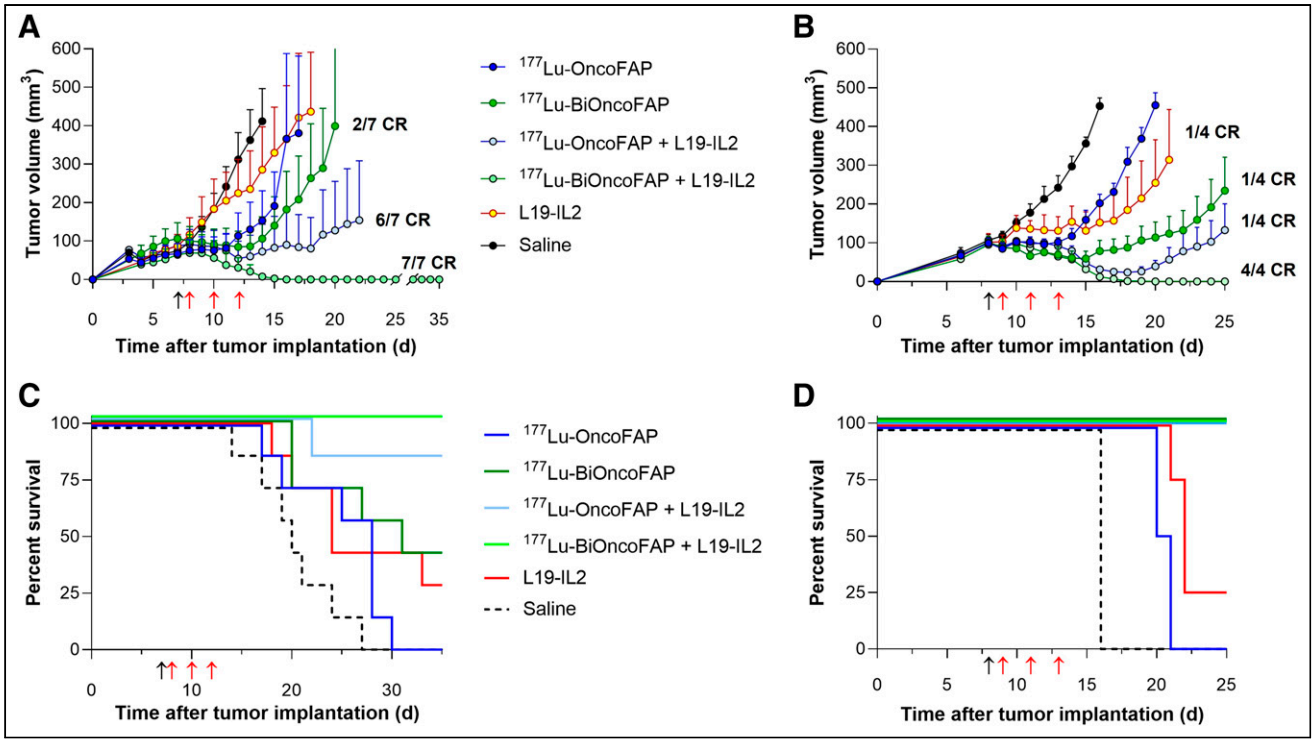


**FIGURE 3.** In vivo therapeutic activity of $^{177}$Lu-OncoFAP or $^{177}$Lu-BiOncoFAP (black arrow), L19-IL2 (red arrows), or their combination in 2 different tumor mouse models (A: HT-1080.hFAP, B: SK-RC-52.hFAP). Efficacy of different treatments was assessed by daily measurement of tumor volumes ($mm^3$). Data points represent mean tumor volume ± SEM. Single mouse plots are reported in Supplemental Figures 6 (HT-1080.hFAP model) and 7 (SK-RC-52.hFAP model). Survival data for HT-1080.hFAP (C) and SK-RC-52.hFAP (D) tumor–bearing mice are presented as Kaplan–Meier plots. Body weight changes of animals treated are presented in Supplemental Figure 8. CR = complete remissions.

remission in all treated animals. No significant body weight loss or other signs of acute toxicity were observed for the different treatments (supplemental materials).

An additional therapy study in the HT-1080.hFAP tumors with 15 MBq/mouse was conducted at 250 nmol/kg (Supplemental Fig. 4).

Statistical analysis of tumor growth values during and after drug administration is presented in Supplemental Tables 4–6.

### Immunofluorescence Analysis

Tumor-bearing mice exposed to the combination of $^{177}$Lu-BiOncoFAP plus L19-IL2 showed a dramatic increase in tumor-infiltrating p46-positive NK cells, as compared with animals treated with vehicle or with single agents (the immunofluorescence results are presented in Supplemental Fig. 5).

### Proteomic Analysis of Tumor Samples After OncoFAP RLT and L19-IL2 Therapy

Proteomic analysis performed on human xenografts (SK-RC-52.hFAP tumor samples) harvested on day 7 after the first injection from mice treated with 5 MBq of $^{177}$Lu-BiOncoFAP (250 nmol/kg), L19-IL2, or their combination allowed study of the impact of different treatments on inflammation in the tumor microenvironment (Figs. 4–6; Supplemental Tables 7–9). Volcano plots presented in Figure 4 show a significant upregulation of murine proteins and downregulation of human proteins in tumor samples from animals treated with L19-IL2 monotherapy (111 upregulated murine proteins and 89 downregulated human proteins), as compared with the saline treatment. The combination with $^{177}$Lu-BiOncoFAP strongly enhanced this proteomic signature (410 upregulated murine proteins and 402 downregulated human proteins). No significant changes in protein abundance were observed for the group treated with $^{177}$Lu-BiOncoFAP monotherapy. An in-depth evaluation of the results presented in Figures 5 and 6 revealed a significant increment of several murine inflammatory proteins after treatment with the combination as compared with the saline group (supplemental materials).

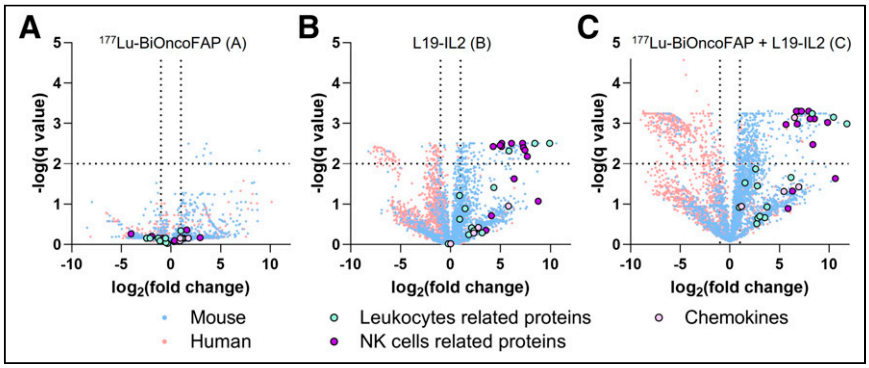


**FIGURE 4.** Quantitative proteomics on SK-RC-52.hFAP tumor samples harvested from mice treated with $^{177}$Lu-BiOncoFAP (A), L19-IL2 (B), or their combination (C). Volcano plots representing up- and downregulated proteins from murine and human origins for each treatment group compare treatment with saline.

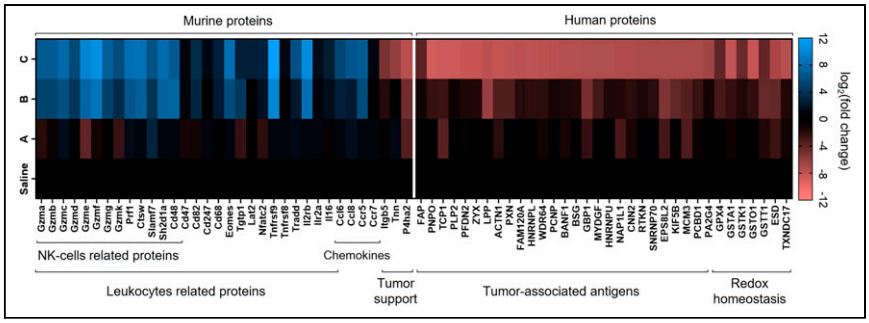


**FIGURE 5.** Cluster heat map of proteomics profiles in different groups. Blue/red jet scale indicates levels of up- or downregulation of different protein entries as compared with vehicle-treated mice. Relative protein abundance is presented as $\log_2$ of fold change.

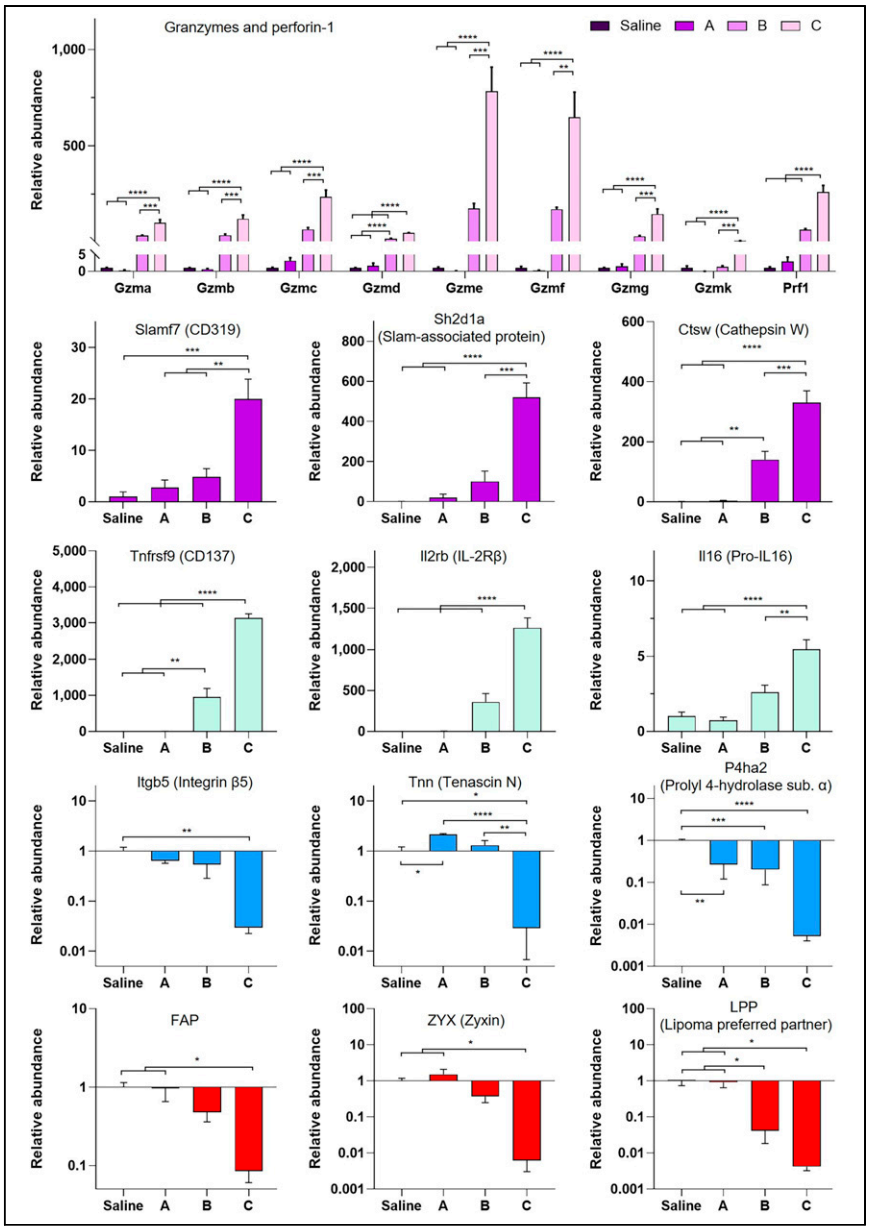


**FIGURE 6.** Statistical analysis (ordinary 1-way ANOVA followed by Bonferroni test) and proteomic data (relative abundance of group A, B, or C as compared with saline) obtained for selection of proteins related to NK cells, leukocytes, tumor microenvironment, and markers of cancer cells. $^{*}P < 0.0332$. $^{**}P < 0.0021$. $^{***}P < 0.0002$. $^{****}P < 0.0001$. ns = $P > 0.1234$.

## DISCUSSION

In this work, the in vivo antitumor efficacy of low-dose OncoFAP RLTs in monotherapy and combination therapy was evaluated in tumor-bearing mice. We observed an enhanced antitumor effect after coadministration of tumor-targeted interleukin 2 (L19-IL2). Activation of NK cells was identified as the cellular source of the observed synergistic treatment effects in the athymic mouse model. The results for targeted radiotherapy nicely complemented the early signs of clinical efficacy for L19-IL2 combination treatments with external-beam radiotherapy (*34,39,40*), which are currently being evaluated in a phase 2 study (*41*).

In previous studies, $^{177}$Lu-BiOncoFAP showed potent in vivo antitumor activity at doses as low as 15 MBq/mouse (*11*). With the aim to appreciate the effect of combination treatments, we have tested $^{177}$Lu-OncoFAP and $^{177}$Lu-BiOncoFAP at even lower activities of 5 MBq/mouse. At these activities, OncoFAP derivatives and L19-IL2 monotherapy led to only minor to moderate suppression of tumor growth. Combination with L19-IL2 drastically enhanced the anticancer efficacy of OncoFAP-based RLTs, leading to complete cures in all mice across both tested tumor models in the case of $^{177}$Lu-BiOncoFAP. The magnitude of increased antitumor effects in combination treatment over monotherapies in our data strongly hint at true synergisms.

Prior mechanistic ex vivo analyses indicated that interleukin 2 potently boosts the anticancer activity of radiotherapeutic modalities through activation of tumor-infiltrating NK cells, CD8-positive T cells, and CD4-positive T cells (*9,32,38,39*). In our study on athymic nude mice, we could define a mechanism of action linked to the activation of NK cells and to a massive release of biocidal granzymes and perforins within the tumor mass. The magnitude of cellular and molecular changes in combination therapy strongly surpassed the sum of effects observed in monotherapies, therefore demonstrating a true synergistic effect. The analysis of the main downregulated proteins clearly described a situation of tumor cell death and regression. We identified a strong downregulation of several well-known tumor markers such as zyxin and its molecular lipoma-preferred partner (involved in focal adhesions of tumor cells to the extracellular matrix), cell-surface proteins such as FAP, enzymes involved in the protumorigenic redox homeostasis (glutathione peroxidase 4, glutathione *S*-transferase A1/K1/O1/T1,

*S*-formylglutathione hydrolase, thioredoxin, and others), and relevant structural proteins of the tumor microenvironment, including tenascin N (tumor cell migration), integrin B5 (matrix adhesion), and prolyl-4-hydrolase (enhancement of collagen deposit). Upregulation of murine pro–interleukin 16, 4-1-BB (CD137, an inducible member of the tumor necrosis factor receptor superfamily and costimulatory T-cell receptor), and the β-subunit of the interleukin 2 receptor illustrate a state of enhanced inflammation in solid tumors after OncoFAP-based RLT/L19-IL2 combination treatment.

Previous studies with $^{177}$Lu-labeled OncoFAP derivatives evaluated biodistribution and tumor uptake at rather high molar amounts of injected ligand (i.e., 125–1,000 nmol/kg) and showed favorable tumor-to-organ ratios with rapid background clearance and negligible uptake in healthy organs. In this work, favorable γ-counter–based biodistribution at high molar amounts of injected ligand could be reproduced by longitudinal SPECT/CT. In contrast, at low molar amounts of injected ligand (3 nmol/kg), the biodistribution was significantly altered for $^{177}$Lu-OncoFAP and $^{177}$Lu-BiOncoFAP, demonstrating relevant background uptake particularly in the skeleton and liver. We speculate that the investigated compounds with very high affinity for FAP (i.e., BiOncoFAP; half-maximal inhibitory concentration, 0.17 nM) (*11*) could be bound to FAP-related molecular targets that are expressed at low levels and therefore saturated at low doses in healthy organs. Similar effects of varying specific activity have been recently observed for prostate-specific membrane antigen ligands (*43,44*), pointing toward the general importance of evaluating investigational radioligands at different molar doses to balance off-target and on-target saturation.

The most relevant limitations of this work consist of the use of athymic immunodeficient mice devoid of functional T lymphocytes but presenting a competent innate immune system and active NK cells. Tumor models used in biodistribution and therapy studies were artificially engineered to express human FAP on the surface of cancer cells. Additional studies on immunocompetent models with high and stromal expression of FAP will be crucial to confirm the mechanism of action of the OncoFAP RLT/L19-IL2 combinations presented here.

## CONCLUSION

In vivo therapy data obtained combining $^{177}$Lu-OncoFAP–based RLTs with targeted delivery of interleukin 2 indicate a strong and synergistic antitumor effect based on the activation of the host immune system in addition to the FAP-mediated radiation effect. This finding warrants clinical trials toward L19-IL2/OncoFAP-based RLT combinations for therapeutic applications in patients with FAP-positive tumors.

## DISCLOSURE

Andrea Galbiati, Ettore Gilardoni, Matilde Bocci, Aureliano Zana, Jacqueline Mock, and Samuele Cazzamalli are employees of Philochem AG, the company that owns and has patented OncoFAP and BiOncoFAP. The Department of Nuclear Medicine of the University Hospital of Münster received an institutional research grant from Philochem AG. No other potential conflict of interest relevant to this article was reported.


## ACKNOWLEDGMENTS

We acknowledge Dr. Stefan Gruber for help in preparing the C-type radiolaboratory, and we acknowledge Dirk Reinhardt, Roman Priebe, Christine Baetza, Sandra Höppner, Irmgard Hoppe, and Alissa Niehues for technical assistance with imaging and therapy experiments.


**KEY POINTS**

**QUESTION:** Does combination with tumor-targeted interleukin 2 enhance the efficacy of FAP-targeted radioligand therapeutics?

**PERTINENT FINDINGS:** A strong in vivo therapeutic synergy was observed when OncoFAP-based RLTs were combined with tumor-targeted interleukin 2 (L19-IL2). Proteomic studies on tumor samples revealed a mechanism of synergistic combination based on the activation of immune cells (NK cells), with a significant enhancement of the expression of granzymes and perforin 1 in the tumor microenvironment.

**IMPLICATIONS FOR PATIENT CARE:** The strong synergy between L19-IL2 and OncoFAP RLTs warrants future clinical trials for this combination for the targeted therapy of solid tumors.

## REFERENCES


1. van den Hoven AF, Keijsers RGM, Lam MGEH, et al. Current research topics in FAPI theranostics: a bibliometric analysis. *Eur J Nucl Med Mol Imaging.* 2023;50:1014–1027.
2. Kratochwil C, Flechsig P, Lindner T, et al. $^{68}$Ga-FAPI PET/CT: tracer uptake in 28 different kinds of cancer. *J Nucl Med.* 2019;60:801–805.
3. Kessler L, Ferdinandus J, Hirmas N, et al. $^{68}$Ga-FAPI as a diagnostic tool in sarcoma: data from the $^{68}$Ga-FAPI PET prospective observational trial. *J Nucl Med.* 2022;63:89–95.
4. Dohi O, Ohtani H, Hatori M, et al. Histogenesis-specific expression of fibroblast activation protein and dipeptidylpeptidase-IV in human bone and soft tissue tumors. *Histopathology.* 2009;55:432–440.
5. Scott AM, Wiseman G, Welt S, et al. A phase I dose-escalation study of sibrotuzumab in patients with advanced or metastatic fibroblast activation protein-positive cancer. *Clin Cancer Res.* 2003;9:1639–1647.
6. Baum RP, Schuchardt C, Singh A, et al. Feasibility, biodistribution, and preliminary dosimetry in peptide-targeted radionuclide therapy of diverse adenocarcinomas using $^{177}$Lu-FAP-2286: first-in-humans results. *J Nucl Med.* 2022;63:415–423.
7. Ferdinandus J, Kessler L, Hirmas N, et al. Equivalent tumor detection for early and late FAPI-46 PET acquisition. *Eur J Nucl Med Mol Imaging.* 2021;48:3221–3227.
8. Backhaus P, Gierse F, Burg MC, et al. Translational imaging of the fibroblast activation protein (FAP) using the new ligand [$^{68}$Ga]Ga-OncoFAP-DOTAGA. *Eur J Nucl Med Mol Imaging.* 2022;49:1822–1832.
9. Millul J, Bassi G, Mock J, et al. An ultra-high-affinity small organic ligand of fibroblast activation protein for tumor-targeting applications. *Proc Natl Acad Sci USA.* 2021;118:e2101852118.
10. Zana A, Galbiati A, Gilardoni E, et al. Fibroblast activation protein triggers release of drug payload from non-internalizing small molecule drug conjugates in solid tumors. *Clin Cancer Res.* 2022;28:5440–5454.
11. Galbiati A, Zana A, Bocci M, et al. A dimeric FAP-targeting small-molecule radioconjugate with high and prolonged tumor uptake. *J Nucl Med.* 2022;63:1852–1858.
12. Ruigrok EAM, van Weerden WM, Nonnekens J, de Jong M. The future of PSMA-targeted radionuclide therapy: an overview of recent preclinical research. *Pharmaceutics.* 2019;11:560.
13. Uccelli L, Boschi A, Cittanti C, et al. $^{90}$Y/$^{177}$Lu-DOTATOC: from preclinical studies to application in humans. *Pharmaceutics.* 2021;13:1463.
14. Zboralski D, Hoehne A, Bredenbeck A, et al. Preclinical evaluation of FAP-2286 for fibroblast activation protein targeted radionuclide imaging and therapy. *Eur J Nucl Med Mol Imaging.* 2022;49:3651–3667.
15. Liu Y, Watabe T, Kaneda-Nakashima K, et al. Fibroblast activation protein targeted therapy using [$^{177}$Lu]FAPI-46 compared with [$^{225}$Ac]FAPI-46 in a pancreatic cancer model. *Eur J Nucl Med Mol Imaging.* 2022;49:871–880.
16. Li H, Ye S, Li L, et al. $^{18}$F- or $^{177}$Lu-labeled bivalent ligand of fibroblast activation protein with high tumor uptake and retention. *Eur J Nucl Med Mol Imaging.* 2022;49:2705–2715.
17. Ferdinandus J, Costa PF, Kessler L, et al. Initial clinical experience with $^{90}$Y-FAPI-46 radioligand therapy for advanced-stage solid tumors: a case series of 9 patients. *J Nucl Med.* 2022;63:727–734.

18. Rao Z, Zhang Y, Liu L, Wang M, Zhang C. [$^{177}$Lu]Lu-FAP-2286 therapy in a case of right lung squamous cell carcinoma with systemic metastases. *Eur J Nucl Med Mol Imaging.* 2023;50:1266–1267.
19. Chan TG, O'Neill E, Habjan C, Cornelissen B. Combination strategies to improve targeted radionuclide therapy. *J Nucl Med.* 2020;61:1544–1552.
20. Thakral P, Sen I, Pant V, et al. Dosimetric analysis of patients with gastro entero pancreatic neuroendocrine tumors (NETs) treated with PRCRT (peptide receptor chemo radionuclide therapy) using Lu-177 DOTATATE and capecitabine/temozolomide (CAP/TEM). *Br J Radiol.* 2018;91:20170172.
21. Twyman-Saint Victor C, Rech AJ, Maity A, et al. Radiation and dual checkpoint blockade activate non-redundant immune mechanisms in cancer. *Nature.* 2015;520:373–377.
22. Pitroda SP, Chmura SJ, Weichselbaum RR. Integration of radiotherapy and immunotherapy for treatment of oligometastases. *Lancet Oncol.* 2019;20:e434–e442.
23. Spetz J, Langen B, Rudqvist N, et al. Hedgehog inhibitor sonidegib potentiates $^{177}$Lu-octreotate therapy of GOT1 human small intestine neuroendocrine tumors in nude mice. *BMC Cancer.* 2017;17:528.
24. Nonnekens J, van Kranenburg M, Beerens CEMT, et al. Potentiation of peptide receptor radionuclide therapy by the PARP inhibitor olaparib. *Theranostics.* 2016;6:1821–1832.
25. Hofving T, Sandblom V, Arvidsson Y, et al. $^{177}$Lu-octreotate therapy for neuroendocrine tumors is enhanced by Hsp90 inhibition. *Endocr Relat Cancer.* 2019;26:437–449.
26. Lundsten S, Spiegelberg D, Raval NR, Nestor M. The radiosensitizer onalespib increases complete remission in $^{177}$Lu-DOTATATE-treated mice bearing neuroendocrine tumor xenografts. *Eur J Nucl Med Mol Imaging.* 2020;47:980–990.
27. Kirichenko AV, Rich TA, Newman RA, Travis EL. Potentiation of murine MCa-4 carcinoma radioresponse by 9-amino-20(S)-camptothecin1. *Cancer Res.* 1997;57:1929–1933.
28. Chen AY, Okunieff P, Pommier Y, Mitchell JB. Mammalian DNA topoisomerase I mediates the enhancement of radiation cytotoxicity by camptothecin derivatives. *Cancer Res.* 1997;57:1529–1536.
29. Pavlakis N, Ransom DT, Wyld D, et al. Australasian Gastrointestinal Trials Group (AGITG) CONTROL NET study: $^{177}$Lu-DOTATATE peptide receptor radionuclide therapy (PRRT) and capecitabine plus temozolomide (CAPTEM) for pancreas and midgut neuroendocrine tumors (pNETS, mNETS)—final results [abstract]. *J Clin Oncol.* 2022;40(suppl):4122.
30. Johannsen M, Spitaleri G, Curigliano G, et al. The tumor-targeting human L19-IL2 immunocytokine: preclinical safety studies, phase I clinical trial in patients with solid tumors and expansion into patients with advanced renal cell carcinoma. *Eur J Cancer.* 2010;46:2926–2935.
31. Hooper AT, Marquette K, Chang CP, et al. Anti-extra domain B splice variant of fibronectin antibody–drug conjugate eliminates tumors with enhanced efficacy when combined with checkpoint blockade. *Mol Cancer Ther.* 2022;21:1462–1472.
32. Moschetta M, Pretto F, Berndt A, et al. Paclitaxel enhances therapeutic efficacy of the F8-IL2 immunocytokine to EDA-fibronectin–positive metastatic human melanoma xenografts. *Cancer Res.* 2012;72:1814–1824.
33. Cazzamalli S, Ziffels B, Widmayer F, et al. Enhanced therapeutic activity of non-internalizing small-molecule-drug conjugates targeting carbonic anhydrase IX in combination with targeted interleukin-2. *Clin Cancer Res.* 2018;24:3656–3667.
34. Schwager K, Hemmerle T, Aebischer D, Neri D. The immunocytokine L19–IL2 eradicates cancer when used in combination with CTLA-4 blockade or with L19-TNF. *J Invest Dermatol.* 2013;133:751–758.
35. Hutmacher C, Gonzalo Núñez N, Liuzzi AR, Becher B, Neri D. Targeted delivery of IL2 to the tumor stroma potentiates the action of immune checkpoint inhibitors by preferential activation of NK and CD8+ T cells. *Cancer Immunol Res.* 2019;7:572–583.
36. Olivo Pimentel V, Marcus D, van der Wiel AMA, et al. Releasing the brakes of tumor immunity with anti-PD-L1 and pushing its accelerator with L19–IL2 cures poorly immunogenic tumors when combined with radiotherapy. *J Immunother Cancer.* 2021;9:e001764.
37. Danielli R, Patuzzo R, Di Giacomo AM, et al. Intralesional administration of L19-IL2/L19-TNF in stage III or stage IVM1a melanoma patients: results of a phase II study. *Cancer Immunol Immunother.* 2015;64:999–1009.
38. Saif A, Rossi AJ, Sarnaik A, Hernandez JM, Zager JS. Efficacy of neoadjuvant intratumoral Darleukin/Fibromun (L19IL2 + L19TNF) in patients with clinical stage IIIB/C melanoma (Neo-DREAM). *Ann Surg Oncol.* 2022;29:3377–3378.
39. Rekers NH, Olivo Pimentel V, Yaromina A, et al. The immunocytokine L19-IL2: an interplay between radiotherapy and long-lasting systemic anti-tumor immune responses. *OncoImmunology.* 2018;7:e1414119.
40. Zegers CML, Rekers NH, Quaden DHF, et al. Radiotherapy combined with the immunocytokine L19-IL2 provides long-lasting antitumor effects. *Clin Cancer Res.* 2015;21:1151–1160.
41. Lieverse RIY, Van Limbergen EJ, Oberije CJG, et al. Stereotactic ablative body radiotherapy (SABR) combined with immunotherapy (L19-IL2) versus standard of care in stage IV NSCLC patients, ImmunoSABR: a multicentre, randomised controlled open-label phase II trial. *BMC Cancer.* 2020;20:557.
42. Jackson P, McIntosh L, Hofman MS, Kong G, Hicks RJ. Technical note: rapid multiexponential curve fitting algorithm for voxel-based targeted radionuclide dosimetry. *Med Phys.* 2020;47:4332–4339.
43. Wurzer A, Pollmann J, Schmidt A, Reich D, Wester H-J, Notni J. Molar activity of Ga-68 labeled PSMA inhibitor conjugates determines PET imaging results. *Mol Pharm.* 2018;15:4296–4302.
44. Tschan VJ, Borgna F, Schibli R, Müller C. Impact of the mouse model and molar amount of injected ligand on the tissue distribution profile of PSMA radioligands. *Eur J Nucl Med Mol Imaging.* 2022;49:470–480.